JOURNAL OF Materials CHEMISTRY

Control of particle growth by chemical transformation in supercritical CO_2/ethanol mixtures

V. Pessey,[a] R. Garriga,[b] F. Weill,[a] B. Chevalier,[a] J. Etourneau[a] and F. Cansell*[a]

[a]*Institut de Chimie de la Matière Condensée de Bordeaux [ICMCB], CNRS-UPR 9048, Université Bordeaux I, 87 Avenue Albert Schweitzer, 33608 Pessac Cedex, France. Fax: 33 (0)5 56 84 27 61; E-mail: cansell@icmcb.u-bordeaux.fr*

[b]*Departamento de Quimica Organica y Quimica Fisica, Facultad de Ciencias, Universidad de Zaragoza, C/Pedro Cerbuna, 50009 Zaragoza, Spain*

Received 24th September 2001, Accepted 9th December 2001
First published as an Advance Article on the web 25th February 2002

The purpose of this work is to take advantage of specific properties of supercritical media to develop a new route for elaboration of fine metal powders. The process consists of the thermal decomposition of a copper precursor previously solubilized in a CO_2/ethanol supercritical mixture.

It has been shown that low initial concentrations of precursor lead to spherical homogeneous nanostructurated particles with a mean size down to below 1 μm, well crystallized, and free from solvent contamination. A decomposition reaction has been performed in a polymer swollen by the supercritical fluid to quench aggregation. Particles sizes in the range 5–20 nm were obtained in polystyrene and in the range 150–250 nm in silicone. Short residence times in a tubular flow reactor (<30 s) allowed non-aggregated nanoparticles to be obtained (particles of size <50 nm were amorphous).

The mechanism of particle growth in supercritical media has been examined assuming both total and partial coalescence (aggregation), since those mechanisms dominate the particle synthesis, according to experimental and simulation results.

1. Introduction

A promising new direction in materials processing is the synthesis of particles that are structured at the nanometer length scale. Subdivision of any material into fine particles leads to high specific surface areas, creating a state of high surface free energy and leading to specific properties for a given system. Optical, magnetic and electrical properties are dramatically sensitive to particle size and shape at this scale.[1] However, significant experimental challenges concern characterization of such materials. The difficulties are not only due to their extremely small sizes, making handling and characterization not trivial, but also due to their very high reactivity with the atmosphere as a consequence of their large area/volume ratio.

A large number of experimental techniques to produce ultrafine particles have been put forward in the literature.[2–7] A glance through recent literature reveals a substantial interest in the physics of tiny metal particles. For instance, unusual mechanical behaviour is observed for submicron-grained copper, in particular, the absence of strain hardening, high plasticity and low strain rate sensivity.[8] Moreover, studies of self-diffusion in nanocrystalline copper have revealed activation energies as much as 40% lower than in conventional polycrystalline copper.[9,10]

Supercritical fluid processes are of increasing interest as reaction media with continuously adjustable properties from gas to liquid (large continuous variations of density, viscosity, diffusivity and solubility of reagents by means of low pressure or temperature modifications).[11,12] In this manner, it is possible to prepare some materials and fine particles at lower pressures and temperatures than those used in classical solid state chemistry.[13] Moreover, for liquid–solid separation techniques, supercritical fluid processing leads to materials free from solvent contamination. Finally, the possibility of using non-high toxicity solvents has contributed to the development of supercritical fluids processing.

The chemical transformation of metallic precursors inside a supercritical fluid is a new route to produce micro-sized homogeneous powders.[14] Acetylacetonates of metals were used as the precursors. UV-visible studies[15] have shown that the optimal molar ratio of CO_2 : ethanol was 80 : 20, since both the solubility of the precursor is enhanced and the precursor decomposition temperature is about 30 K lower than in pure CO_2. Furthermore, the critical coordinate of this mixture (T_c = 365 K, P_c = 14.5 MPa[16]) is not dramatically increased. We have shown, in a previous study,[13] that the decomposition of bis(hexafluoroacetylacetonate)copper(II) hydrate (Cu(hfa)$_2$·H_2O) in a CO_2/ethanol mixture, at T = 473 K and P = 19 MPa, leads directly to spherical copper particles free of solvent.

In this work, the effect of different experimental parameters on the size and the morphology of the final particles is investigated. These parameters are: initial concentration of precursor, temperature, viscosity, residence time. Two processes have been used: a batch synthesis or a continuous mode. Based on the experimental observations, a numeric simulation is proposed in order to highlight the mechanisms which dominate particle growth of the nanoparticles in supercritical fluid media.

2. Experimental

The metallic precursor was provided by Sigma-Aldrich and used without further purification. The supercritical grade CO_2 was used as received from the commercial supplier Air Liquid and the absolute ethanol (R. P. NORMAPUR™ Analytical Reagent) was delivered by Prolabo.

 DOI: 10.1039/b108670g

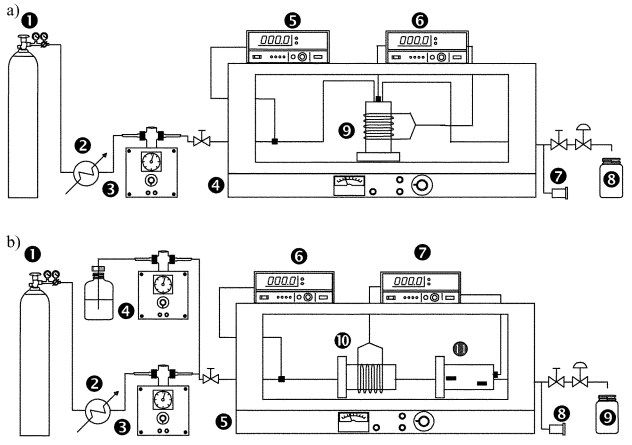

Fig. 1 Apparatus for particles elaboration in (a) the batch process (1, solvent source; 2, cooler; 3, pump; 4, hot-air oven; 5, pressure sensor; 6, temperature regulator; 7, contact breaker; 8, solvent trap; 9, reactor) and (b) continuous process (1, solvent source; 2, cooler; 3, pump; 4, solution of $Cu(hfa)_2 \cdot H_2O$ in ethanol; 5, hot-air oven; 6, pressure sensor; 7, temperature regulator; 8, contact breaker; 9, solvent trap; 10, reactor; 11, high pressure cell with TEM grids).

2.1. Batch process

The high pressure and high temperature experimental set up (Fig. 1(a)) was described elsewhere.[13] The reactor is made of 316 stainless steel with an external heating source which allows the precursor decomposition temperature to be attained. A polytetrafluoroethylene film (PTFE, thickness = 0.25 mm) covers the inside the reactor to avoid contamination of the wall of the cell. The system itself is placed in an hot-air oven. Two thermocouples measure the temperature, one inside the hot-air oven and the other inside the reactor. The high pressure generator is a fluid metering pump (CM 3200 P/F) which permits the introduction of CO_2.

A known and variable amount of precursor was dissolved in 4.5 cm^3 of ethanol in the reactor (V = 20 cm^3). CO_2 was pumped in to obtain a CO_2/ethanol mixture in molar proportion 80/20. The hot-air oven was then heated in order to solubilize the precursor in the supercritical medium. The temperature was then fixed at 473 K (since in our working conditions the decomposition temperature is 468 K[15]), and the pressure was maintained constant at 19 $\pm$ 0.5 MPa for 1 h. The precursor decomposition leads to precipitation of copper particles in the reactor. The organic part of the precursor is still soluble in the supercritical fluid and is easily removed when the vessel is vented and trapped at the outlet of the installation. After returning to ambient conditions the copper particles were directly recovered free from solvent and organic contaminants.

Some different experiments were carried out in order to study the effects of noticeably different reaction media viscosities. A polymer which can be swollen by the CO_2/ethanol supercritical mixture was used as the reaction medium and the experimental protocol was changed as follows: a quantity of polymer was mixed with a known quantity of precursor and introduced in a glass pill box (12 mm $\times$ 45 mm). The CO_2/ethanol (80/20) supercritical mixture mixture was allowed to fill the reactor which was heated to 423 K. The pressure was maintained at 15 MPa for 12 h during which the polymer was swollen by diffusion of the supercritical mixture. After this, the decomposition reaction was performed at the usual working conditions (473 K, 19 MPa, 1 h) and then the system was slowly decompressed at 473 K (some MPa h^{-1}, by controlling the bubble flow at the end of the pipe) in order to extract the CO_2/ethanol/organic part of the mixture of the precursor and to avoid the "sponge" phenomenon (this corresponds to the fact that CO_2, which swells the polymer matrix at 25 MPa, is transformed by decompression into bubbles in the polymeric matrix). When atmospheric pressure was reached the installation was cooled to room temperature. Polystyrene (molar mass = 5000 g mol^{-1}) and silicone (polydimethylsiloxane, molar mass = 35 000 g mol^{-1}) were chosen because the supercritical CO_2/ethanol mixture easily swells them. Furthermore, they exhibit a vitreous transition temperature lower than the decomposition temperature of the precursor, they are not degraded at the working temperature and they showed a large range of viscosity (Table 1).

2.2. Continuous process

Since batch reactors do not allow flash reactions to be performed (because of the thermal inertia of the reactor) a tubular flow reactor was used. Several residence times were used for the same initial concentration of precursor in the CO_2/ethanol mixture. The previous experimental set up was modified as shown in Fig. 1(b). The high pressure generator is a fluid metering pump (miniPump Duplex, 2396-47) which introduces both the CO_2 and a solution of precursor dissolved in ethanol (30 g l^{-1}, prepared prior to use), at variable flow rates, in the molar proportion CO_2 : ethanol = 80 : 20. The decomposition reaction occurs inside the reactor which is maintained at 473 K and 19 MPa. Some of the particles generated in the reactor are small enough to be dragged by the flowing fluid to a second vessel placed at the outlet of the reactor, and are deposited on grids used for transmission electron microscopy (TEM) observation.

A previous study has shown that in this continuous process the hydrodynamics of our reactors is of piston flow type.[15] In this case, the residence time (t_r) can be calculated by the following expression:

$$t_r = (\text{reactor volume}) \times (\text{density of the supercritical mixture}) \times (1/\text{mass flow})$$

here the mass flow corresponds to the quantity, in g, of solvent + precursor per second, which passes through the reactor.

2.3 Characterization of samples

The samples were characterized by conventional X-ray powder diffraction (Cu Kα radiation). The particle size and morphology were investigated by scanning electron microscopy (SEM) using a JEOL 840 microscope and by transmission electron microscopy (TEM) by means of a JEOL 2000 FX microscope. The particle sizes and particle size distribution were determined by manual counting.

3. Results

3.1 Bacth process

3.1.1 Influence of precursor concentration. The knowledge of the initial concentration of the metallic precursor allows control of the amount of copper released in the decomposition reaction and therefore the size and size distribution of the particles obtained.

Fig. 2 shows the influence of precursor concentration on both the morphology and the size of the particles. Table 2, which summerizes the mean size of the particles *versus* the

Table 1 Viscosity values at 473 K and 20 MPa of supercritical CO_2 and polymers swollen by supercritical CO_2

	Viscosity, η/Pa s	Ref.
CO_2	2.9×10^{-5}	17
Silicone	10^{-3}–10^{-4}	18, 19
Polystyrene	2	20

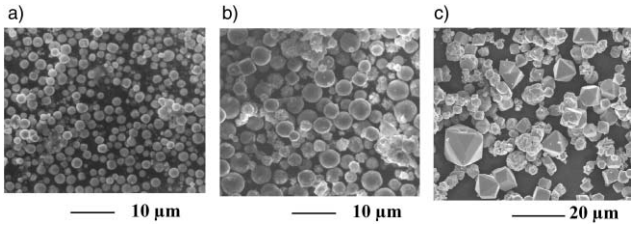

Fig. 2 SEM pictures of particles obtained with various initial precursor concentrations (g g^{-1}): (a) 10^{-2} (sample III), (b) 4.1×10^{-2} (sample V), (c) 4.2×10^{-1} (sample IX).

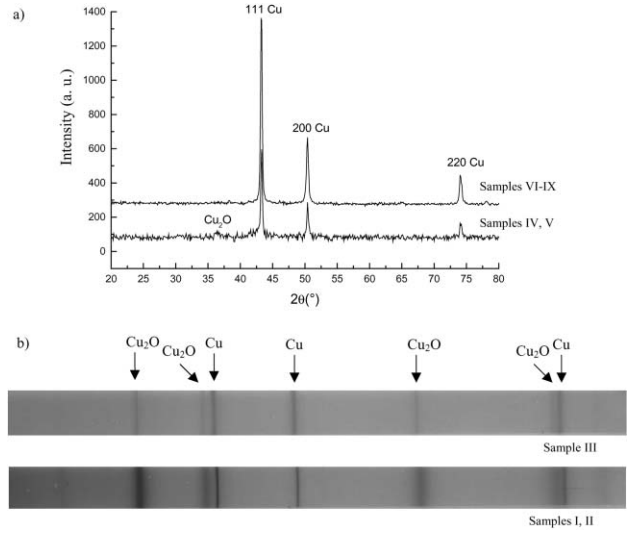

Fig. 3 X-Ray diffraction patterns relating to samples described in Table 2.

precursor concentration, shows that a decrease of the concentration leads to a decrease of the particles size.

The X-ray diffraction patterns (Fig. 3) indicate the formation of metallic copper and/or copper oxide particles. When the samples are manipulated in the air atmosphere the smallest copper particles are probably oxidized.

Two families of particles can be distinguished (Table 2 and Fig. 2).

First, those obtained with initial precursor concentrations between 8.4×10^{-3} and 4.1×10^{-2} g g^{-1} (g of precursor per g of solvent). The particles are spherical and apparently smooth (Figs. 2(a) and (b)). SEM study of surfaces indicates aggregation of nanosized particles (Fig. 4). As will be discussed later, oxide formation is attributable to this nanostructured organization with large surface/volume ratio. The average radius of these particles decreases with decreasing initial

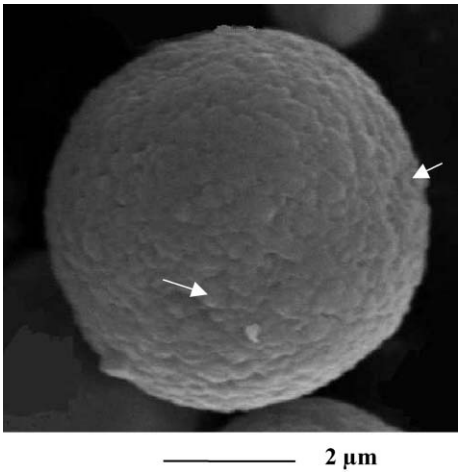

Fig. 4 SEM image of the surface of a nanostructured particle obtained in experiment V (Table 2).

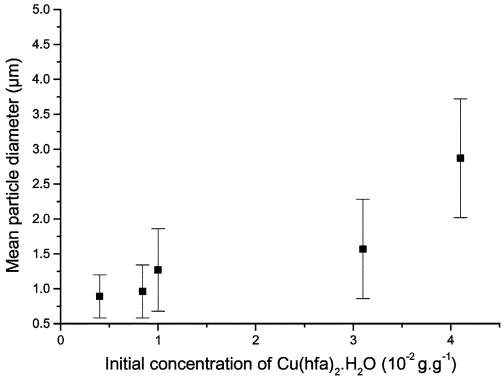

Fig. 5 Evolution of the average particle diameter as a function of the initial precursor concentration.

concentration of the precursor and the size distribution becomes narrower (Fig. 5). However for $Cu(hfa)_2 \cdot H_2O$ concentrations lower than 3×10^{-2} g g^{-1}, the decrease in size is not significant, and thus the batch process is not an adequate route to obtain ultra-fine particles.

Secondly, the particles obtained from concentrations of precursor varying between 5.1×10^{-2} and 4.2×10^{-1} g g^{-1}, exhibit a particular morphology : a new population of pronounced facetted shapes appears corresponding to typical ffc copper (Fig. 2(c)). SEM images (Fig. 6b) show that particles consist of micro-sized strongly aggregated particles (>500 nm). The samples are heterogeneous in morphology and consequently the medium diameter of particles cannot be defined.

Table 2 Effects of initial precursor concentrations on particle synthesis in a batch reactor (working conditions: 473 K, 19 MPa, 1 h)

Experiment	Concentration/ g g^{-1}	Average diameter/µm	Standard deviation/µm	Number of particles analysed	Phase analysis[a]	Morphology
I	4×10^{-3}	0.89	0.31	323	Cu, Cu_2O	Spherical particles *via* nanocrystal aggregation
II	8.4×10^{-3}	0.96	0.38	487	Cu, Cu_2O	Spherical particles *via* nanocrystal aggregation
III	1.0×10^{-2}	1.27	0.59	417	Cu, Cu_2O	Spherical particles *via* nanocrystal aggregation
IV	3.1×10^{-2}	1.57	0.72	522	Cu, traces of Cu_2O	Spherical particles *via* nanocrystal aggregation
V	4.1×10^{-2}	2.87	0.85	184	Cu, traces of Cu_2O	Spherical particles *via* nanocrystal aggregation
VI	5.1×10^{-2}	—	—	—	Cu	No smooth spherical particles
VII	1.0×10^{-1}	—	—	—	Cu	Two population of particles: spherical and polyhedra
VIII	2×10^{-1}	—	—	—	Cu	Two population of particles: spherical and polyhedra
IX	4.2×10^{-1}	—	—	—	Cu	Spherical particles have disappeared. Several types of polyhedra

[a]Phase analysis of samples was performed by X-ray powder diffraction.

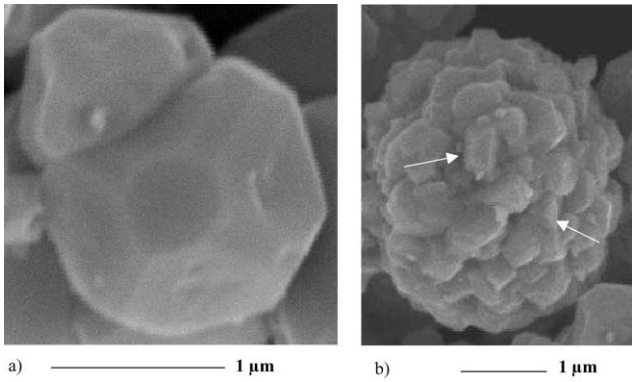

Fig. 6 SEM images of particles obtained for high initial precursor concentrations: experiment IX (a) and VIII (b) (the particles result from the aggregation of submicronic crystallites).

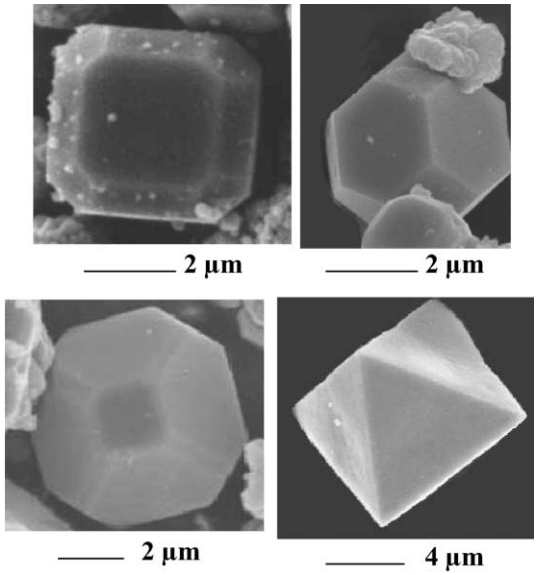

Fig. 7 Different shapes of crystalline particles observed in experiment IX.

It can be noted, that the larger the initial $Cu(hfa)_2 \cdot H_2O$ concentration, the larger the particles. Some geometric shapes (octahedra) are obtained at high concentrations of precursor (4.2×10^{-1} g g^{-1}) (Fig. 7).

3.1.2 Influence of temperature. The increase of temperature, from 473 to 573 K, takes about 15 minutes in our experimental set up. We consider that the temperature rise from 473 to 573 K does not modify the precursor decomposition kinetics, as has been shown previously[15] (the reaction of decomposition at 473 K is almost complete (90%) after 4 min and the half-life time of the decomposition reaction is 70 s). Thus, this experiment allows the study of the effect of a thermal treatment on the copper particles up to 573 K. The used initial concentration of metallic precursor to check the effect of the temperature was 10^{-2} g g^{-1} (sample III).

The X-ray diffraction pattern (Fig. 8(a)) reveals only the presence of metallic copper: the Cu_2O previously observed at 473 K is no longer detectable. Moreover, the thermal treatment at 573 K introduces two major modifications:

(1) A disappearance of nanostructured spherical particles. In fact, after the thermal treatment, the particles consist of aggregates of submicronic particles. In this case, the surface reactivity of the particles is reduced. As a consequence, the particles are clearly less sensitive to air oxidation.

(2) The presence of micronic particles showing a necklace like structure (Fig. 8b).

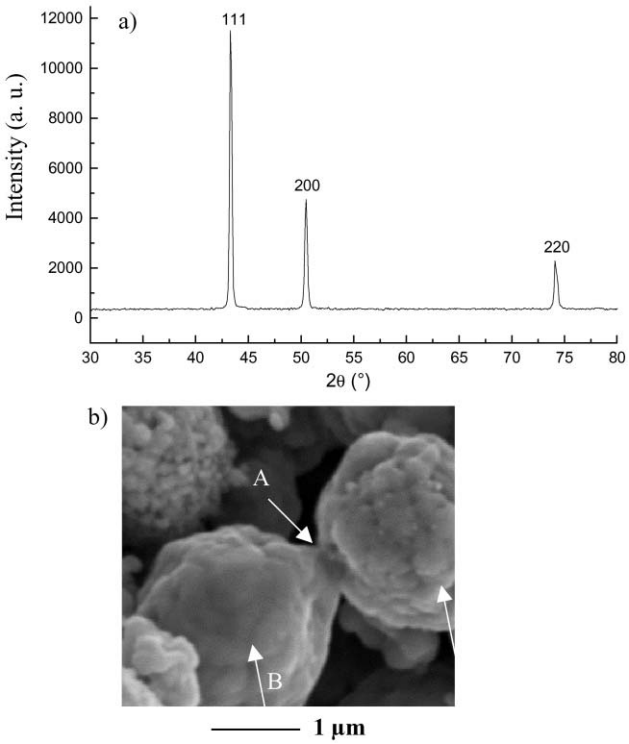

Fig. 8 (a) X-Ray diffraction pattern of the powder obtained after a thermal treatment at 573 K. (b) SEM image of copper powder obtained after a thermal treatment at 573 K. Arrow "A" shows the neck formation between two particles while arrow "B" shows the modification of the particle structure.

3.1.3 Influence of the viscosity of the reaction medium. The effect of the viscosity of the media on the size of the particles is illustrated in Figs. 9 and 10. Obviously an increase of the viscosity of the medium leads to a decrease of the grain size. The electron diffraction pattern of the particles grown in a polystyrene matrix shows the presence of copper as well as copper oxide (Fig. 9). The formation of copper oxide may be understood if the very small size of the particles is considered.

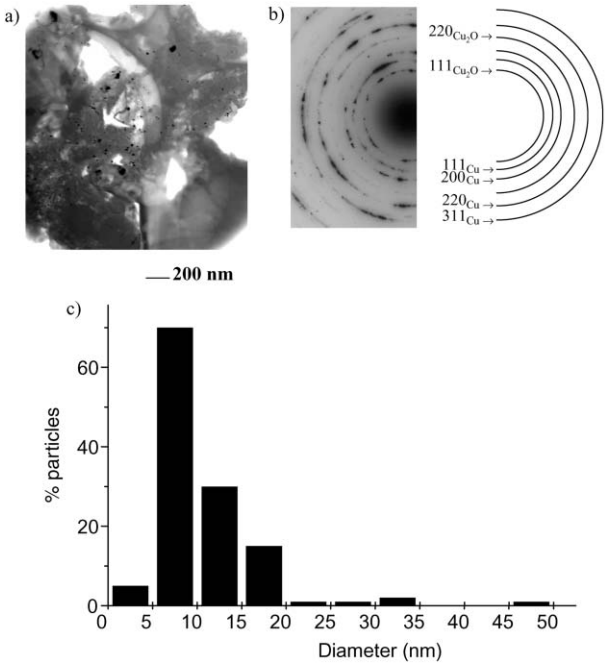

Fig. 9 TEM image obtained in dark field (a), electron diffraction pattern (b) and size distribution (c) of fine particles dispersed in a polystyrene matrix.

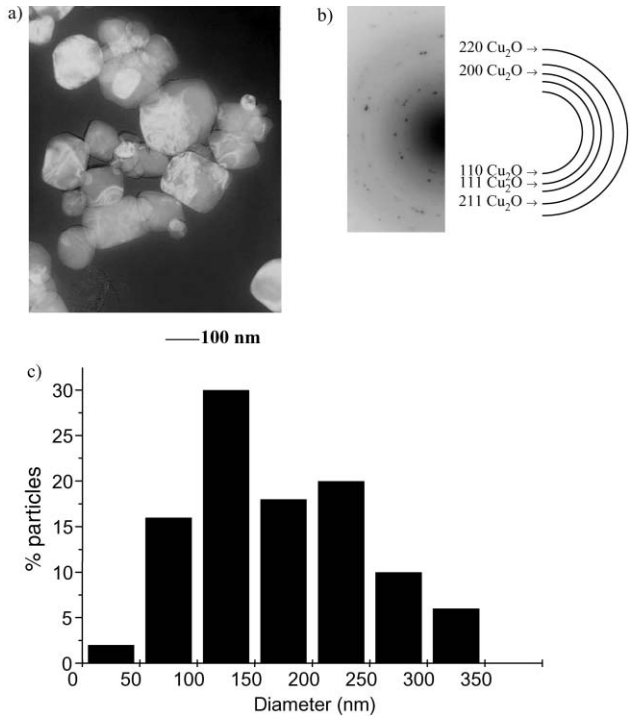

Fig. 10 TEM image (a), electron diffraction pattern (b) and size distribution (c) of particles obtained by $Cu(hfa)_2 \cdot H_2O$ decomposition in silicone swollen by the supercritical mixture CO_2/ethanol (80/20).

In the silicone, even if the size of the particle is larger, electron diffraction only reveals the presence of copper oxide (Fig. 10). This result is not surprising since oxygen is slightly soluble in the silicone.

3.2 Continuous process

Four residence times have been used: t_r = 0.35, 6, 12 and 24 s. In each experiment the recovery vessel was thermostatted at 303 K. Fig. 11(a) (corresponding to t_r = 0.35 s) shows amorphous materials, the particle size ranging between 10 and 50 nm. In Fig. 11(b) (t_r = 6 s) homogeneous well crystallised particles appear to be copper and copper oxide, with diameters between 200 and 350 nm. For larger residence times (t_r = 12 and 24 s, Figs. 11(c) and (d), respectively), heterogeneous morphologies and granulometries of pure copper particles (average size between 25 and 250 nm) are obtained.

4. Discussion

To understand the mechanism which governs the particle growth, we must examine each of growth steps involved

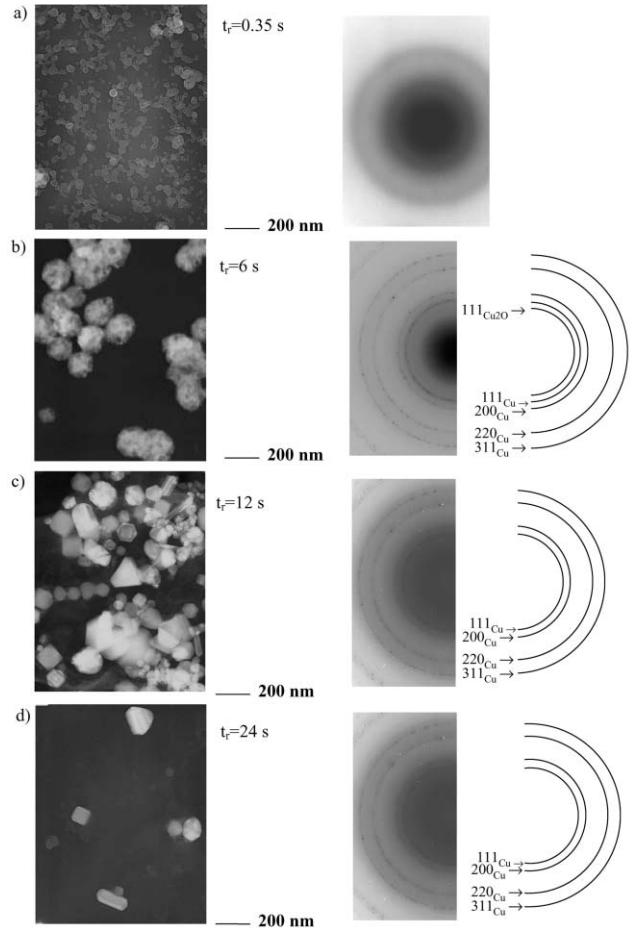

Fig. 11 TEM images and electron diffraction patterns showing the influence of residence time on particle elaboration in the continuous process.

(Fig. 12). The kinetics of the decomposition reaction of $Cu(hfa)_2 \cdot H_2O$ has already been studied:[15] it leads to rapid and extreme supersaturation of copper, and thus, generation of utra-fine particles of copper with sizes estimated to the order of atomic dimensions.[17] The primary particles grow both by binary contact (due to Brownian movement) and then coalescence of ultra-fine particles (liquid-like coalescence). It has been found that the time for the coalescence of two metal particles is proportional to the fourth power of the radius and to the diffusion coefficient of the metal which is directly connected to the working temperature.[17] When these primary particles grow, the particle mobility and excess surface free energy decrease, leading to a decreasing of particle coalescence. Thus, the particles mainly grow *via* aggregation (partial

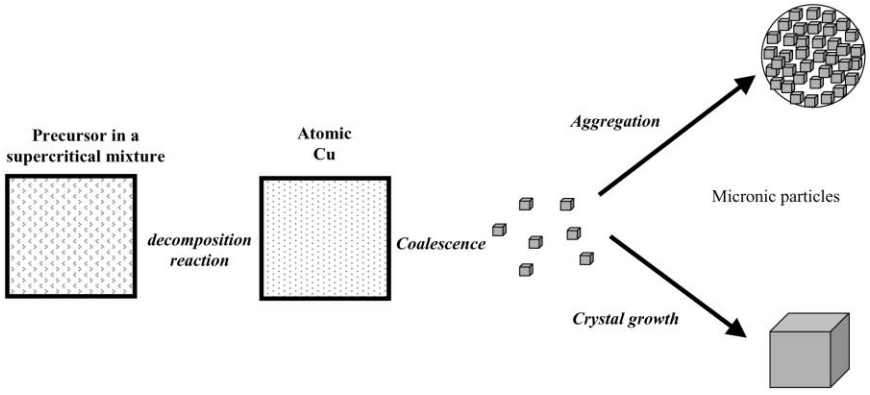

Fig. 12 Schematic representation of particle formation in supercritical conditions.

coalescence). The structure of the resulting micron sized particles may be denoted as nano-structured, since final particles are formed by primary nano-particles, as can be clearly seen in Fig. 4.

These different steps of the growth can be pointed out by modifying the operating synthesis conditions.

(1) For very low concentrations of copper precursor ($<1 \times 10^{-2}$ g g^{-1}) only a limited number of ultra-fine particles are formed in a limited time (Fig. 2). A complete coalescence of these ultra-fine particles occurs leading to small crystal particles which lead by aggregation to spherical and smooth particles (Fig. 4).

(2) For higher concentrations ($>1 \times 10^{-1}$ g g^{-1}) the production of ultra-fine particles occurs during a longer time. As previously discussed, these ultra-fine particles form primary particles which can grow by coalescence with other ultra-fine particles produced (Fig. 7). This mechanism leads to larger final particle sizes. As there is still formation of ultra-fine particles in the presence of these larger particles, an increase of the distribution of the particle sizes is observed. Moreover, formation of polycrystalline particles occurs by partial coalescence of larger particles (Fig. 6).

(3) For low values of residence time (<1 s) it is possible to stop the aggregation phenomena and obtain only the primary particles (Fig. 11a). Thus, aggregation phenomena can be controlled by the value of the residence time (Figs. 2 and 11).

(4) When the viscosity of the medium is increased the extent of aggregation is decreased and can be completely suppressed for higher viscosity values (2 Pa s). Clearly, the viscosity of the reacting medium permits the control of the aggregation step of the growth mechanism.

In order to validate this representation of particle formation in supercritical conditions, a numeric simulation of the evolution of the particle size *versus* time has been performed allowing a comparison with the experimental results.

5. Numeric simulation

We have attempted to simulate the growth of the primary particles making up the aggregates (Appendix). In the simulation, the precursor decomposition reaction is assumed to be instantaneous and we consider liquid-like coalescence of particles as the dominant growth mechanism. The aggregation mechanism is not taken into account. The numerical model is based on the influence of the diffusion coefficient on the particle size (Stokes–Einstein relation):

$$D = \frac{kT}{6\pi R\eta} \quad (1)$$

Here D is the particle diffusion coefficient, k the Boltzmann constant, T the temperature, r the particle radius and η the medium viscosity.

We assumed that particles are animated by Brownian movement:

$$\langle x^2 \rangle = 2Dt \quad (2)$$

where $\langle x \rangle^2$ is the mean free path, and t the time.

The assumptions are:

(1) Particle coalescence occurs by binary contact.

(2) Particle coalescence occurs on a time scale shorter than the time between collision events.

(3) Particles are spherical.

(4) Each collision between two spherical particles is effective (total coalescence) and gives a larger spherical particle.

(5) Particle distribution in the reactor is homogeneous.

(6) The precursor is instantaneously decomposed to copper.

Results of the calculated sizes in the case of growth in supercritical CO_2 are plotted in Fig. 13 as a function of time. After 1 h in the reactor, the calculated particle radius is 1.21 μm, which should be compared with the experimental value of sample IV in Table 2 of 1.57 μm. Fig. 13 shows clearly that, the shorter is the residence time, the smaller is the particle size. The particle size increases rapidly over short time ranges and smoothly for larger times.

These results are in agreement with particle sizes obtained in the continuous process. For short values of residence time (t_r = 0.35 s), the average radius size is between 10 and 50 nm. Thus the increase of the residence time values from t_r = 6 to 24 s leads to a significant increase of the particle size.

From this analysis, it is seen that calculated particle size is underestimated by the calculation, since the model simply involves growth prior to the onset of aggregation. The abrupt transition of the evolution of the particle size when aggregation starts has already been pointed out.[22]

Fig. 14 and Table 3 show the effect of viscosity on particle size. Experimental and calculated values are of the same order of magnitude. The smaller the viscosity of the medium the larger is the particle size. In the case of polymers, the calculations did not take into account the fact that the real precursor concentration inside the polymer swollen by supercritical fluid was smaller than the weigthed quantity.

The lack of physico-chemical data for our solvent–solute system does not allow application of a more sophisticated simulation.

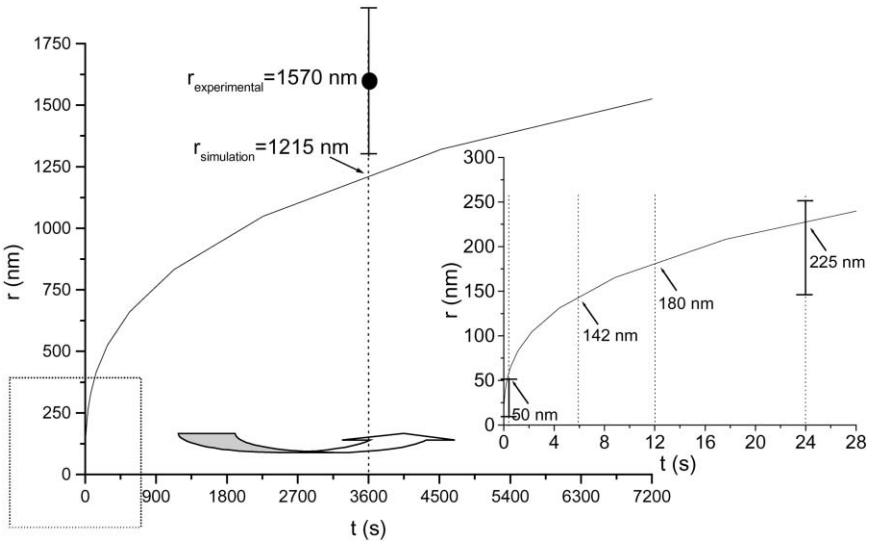

Fig. 13 Comparison between experiment and numeric simulation of the growth of particles in supercritical CO_2.

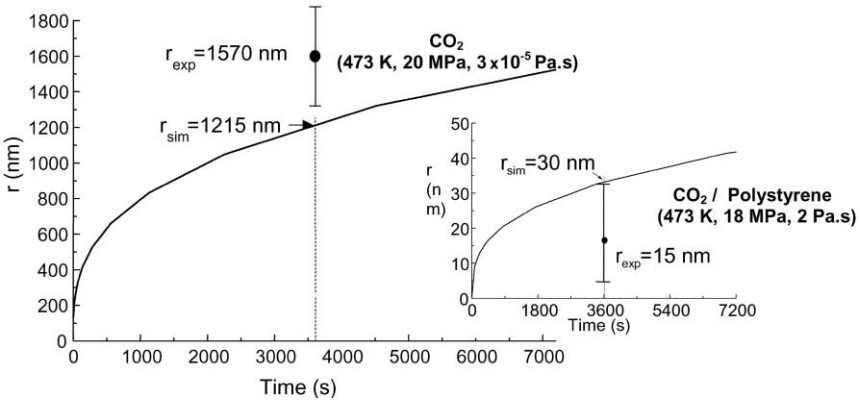

Fig. 14 Influence of the reaction medium viscosity on the average radius of the particles; comparison between the numeric simulation and the experiment

Table 3 Comparison of experimental particle sizes and calculated values in CO_2, silicone and polystyrene (viscosity values were taken from Table 1: $\eta[CO_2] = 2.9 \times 10^{-5}$ Pa s, η[silicone] = 10^{-3}–10^{-4} Pa s, η[polystyrene] = 2 Pa s)

Viscosity, η/Pa s	r_{exptl}/nm	r_{calc}/nm
$<10^{-5}$	>15	>10
10^{-4}–10^{-3}	400–800	150–250
$>10^{-2}$	<100	<50

6. Conclusions

The aim of this work was to study the influence of some of the experimental parameters of the thermal decomposition of a copper precursor in supercritical media for producing material powders.

The initial concentration of the precursor has been found to have an influence on the size as well as on the morphology of the particles. Low initial concentrations lead to spherical nanostructured micronic particles while with higher concentrations polyhedral particles are obtained.

The viscosity of the supercritical media and residence time have an influence on the aggregation of the particles. Nanometric particles can be obtained for media of high viscosity (*e.g.* polystyrene) or for low residence time in the reactor.

A numerical simulation of the size of the particle *versus* the time of synthesis has been proposed and we have shown that it can aid in predicting the order of magnitude of the particle sizes.

7. Appendix

Initial data required for the calculations are: mass of precursor (m), viscosity (η) and volume (V) of the medium. Calculations have been performed for $m = 0.060$ g; viscosity values were taken from Table 1: $\eta[CO_2] = 2.9 \times 10^{-5}$ Pa s, η[silicone] = 10^{-3}–10^{-4} Pa s, η[polystyrene] = 2 Pa s; the reactor volume in the case of CO_2 has been taken equal to 2 cm^3, and in the case of polymer, the quantity introduced corresponded approximately to 1.30 cm^3.

First, the number of copper atoms available in the medium, nat, is calculated (the precursor decomposition reaction and nucleation step are assumed to be instantaneous, since, as discussed above, the coalescence in the beginning is very rapid and the last steps will govern the process):

$$\mathrm{nat} = mN_A/M \quad (1)$$

where N_A is the Avogadro constant and M is the molecular weight (495.66 g mol^{-1}).

Second, at each step i, the programme calculates the number of atoms inside a particle:

$$\mathrm{nat}_{ins}[i] = 2^i \quad (2)$$

(For instance, in the beginning ($i = 0$), each particle consists of 2^0 atoms; in the following step ($i = 1$), all two copper atoms coalesce (completely) to form particles with $\mathrm{nat}_{ins}[1] = 2^1$; for $i = 2$, these particles coalesce two by two to form spherical particles with $\mathrm{nat}_{ins}[2] = 2^2$, and so on).

At each step i, the number of particles obtained can be calculated as follows:

$$n[i] = \frac{\mathrm{nat}}{\mathrm{nat}_{ins}[i]} \quad (3)$$

and since

$$\mathrm{nat}_{ins} = \frac{4/3\pi(r[i])^3}{4/3\pi(r_{Cu})^3} \quad (4)$$

where r_{Cu} stands for the copper atomic radius 1.28 Å, the particle's radius can be obtained by means of the following equation:

$$r[i] = 1.28\sqrt[3]{\mathrm{nat}_{ins}[i]} \quad (5)$$

The diffusion coefficient is calculated by the Stokes–Einstein relation:

$$d[i] = \frac{kT}{6\pi r[i]\eta} \quad (6)$$

with k the Boltzmann constant, and $T = 498$ K.

The mean volume available for each particle is:

$$\mathrm{vp}[i] = \frac{V}{n[i]} \quad (7)$$

and the mean distance between two particles is:

$$\langle x[i]\rangle = \sqrt[3]{\mathrm{vp}[i]} - 2r[i] \quad (8)$$

Assuming Brownian movement, the time for two particles (with a diffusion coefficient $d[i]$) to meet can be calculated as:

$$t[i] = \frac{\langle x[i]^2\rangle}{2d[i]} \quad (9)$$

where $\langle x[i]^2\rangle$ is the mean free path of the particles.

Finally, the time to obtain a particle of size $r_{part}[i]$ (from the beginning) is:

$$t_{total}[i] = \sum_{j=0}^{i-1} t[j] \quad (10)$$

Therefore, $t_{total}[i]$ values can be plotted *versus* $r_{part}[i]$ values (Fig. 14).

Acknowledgement

We gratefully acknowledge financial support from Ministerio de Educacion y Cultura (Spain) through Grant No. PF99 0025447316, from Région Aquitaine, and from CNRS.

References

1 M. T. Gacoin, *GALERNE 98. De la Molécule au Solide*. La Rochette, 4–9 October, 1998, p. 87.
2 R. Uyeda, *Prog. Mater, Sci.*., 1991, **35**, 1.
3 L. M. Sheppard, *Solid State Commun.*, 1989, **68**, 979.
4 D. W. Johnson, *Ceram. Bull.*, 1981, **60**, 221.
5 P. Cousin and R. A. Ross, *Mater. Sci. Eng. A*, 1990, **130**, 119.
6 E. R. Buckle and P. T. Tsakiropoulos, *Int. Met. Rev.*, 1986, **31**, 258.
7 J. H. Fendler and F. C. Meldrum, *Adv. Mater.*, 1995, **7**, 607.
8 R. Z. Zaliev, E. V. Kozlov, F. Yu, J. Lian, A. A. Nazarov and B. Baudelet, *Acta Metall. Mater.*, 1994, **42**, 2467.
9 J. Horvath, J. Birringer and H. Gleiter, *Solid State Commun.*, 1987, **62**, 319.
10 W. Dickenscheide, R. Birringer, H. Gleiter, O. Kanert, B. Michel and B. Gunther, *Solid State Commun.*, 1991, **79**, 683.
11 *Supercritical Fluids–Fundamentals for Application*, ed. E Kiran and J. M. H. Levelt Sengers, Nato ASI ser. E 273, Kluwer, Dordrecht, 1994.
12 (*a*) F. Cansell, S. Rey and P. Beslin, *Rev. Inst. Fr. Pét.*, 1998, **53**, 71; (*b*) F. Cansell, B. Chevalier, A. Demourgues, J. Etourneau, Ch. Even, Y. Garrabos, V. Pessey, S. Petit, A. Tressaud and F. Weill, *J. Mater. Chem.*, 1999, **9**, 67.
13 (*a*) T. Adschiri, K. Kanazawa and K. Arai, *J. Am. Ceram. Soc.*, 1992, **75**, 2615; (*b*) V. Pessey, R. Garriga, F. Weill, B. Chevalier, J. Etourneau and F. Cansell, *High-Pressure Res.*, 2001, **20**, 289; (*c*) A. Cabanas and M. Poliakoff, *J. Mater. Chem.*, 2001, **11**, 1408.
14 R. M'Hamdi, J. F. Bocquet, K. Chhor and C. Pommier, *J. Supercrit. Fluids*, 1991, **4**, 55.
15 R. Garriga, V. Pessey, F. Weill, B. Chevalier, J. Etourneau and F. Cansell, *J. Supercrit. Fluids*, 2001, **20**, 55.
16 H. Pöhler and E. Kiran, *J. Chem. Eng. Data.*, 1997, **42**, 384.
17 N. B. Vargaftik, *Tables on the thermophysical properties of liquids and gases in normal and dissociated states*, J. Wiley, New York, 2nd edn., 1975, p. 207.
18 Y. Xiong and E. Kiran, *Polymer*, 1995, **36**, 4817.
19 R. Mertsch and B. A. Wolf, *Macromolecules*, 1994, **27**, 3289.
20 F. Cansell, personal communication.
21 A. R. Thölén, *Acta Metall.*, 1979, **27**, 1765.
22 R. C. Flagan and M. M. Lunden, *Mater. Sci. Eng. A*, 1995, **204**, 113.